Springer

KSME

Journal of Mechanical Science and Technology 32 (3) (2018) 1287~1296
www.springerlink.com/content/1738-494x(Print)/1976-3824(Online)
DOI 10.1007/s12206-018-0233-6

3D Monte Carlo simulation of grain growth in friction stir welding †

Z. Zhang[1,2,*] and C. P. Hu[1]

[1]*State Key Laboratory of Structural Analysis for Industrial Equipment, Department of Engineering Mechanics, Faculty of Vehicle Engineering and Mechanics, Dalian University of Technology, Dalian, 116024, China*
[2]*International Research Center for Computational Mechanics, Dalian University of Technology, Dalian, 116024, China*

(Manuscript Received April 21, 2017; Revised August 29, 2017; Accepted October 31, 2017)

Abstract

The 3D fluid model was used to simulate the friction stir welding process. Three-dimensional Monte Carlo model with nucleation in each MC step was then applied to simulate the grain growth. The validity of this model is verified by comparison with the experimental and numerical results. The influences of tool shoulder diameter and rotational speed are further studied. Equiaxed grains in the stirring zone are increased with the increase of the diameter and the rotation speed of the shoulder. The grain sizes tend to be more uniform from retreating side to advancing side when the rotational speed or shoulder diameter is increased.

Keywords: Friction stir welding; Grain growth; Monte Carlo method; Fluid turbulence model

1. Introduction

Friction stir welding (FSW) is an important solid-state joining technique invented in 1991, and which is widely used in industrial fields [1, 2]. In FSW, a rotation tool will be inserted into the joining line and traversed with rotations. The frictional heat generated by the welding tool softens the surrounding material. The material around the welding tool can be then stirred. The material flow patterns are different between the advancing side and the retreating side. Detailed information on material flow has been clearly described in both experiments [3, 4] and numerical simulations [5, 6]. The friction stir weld can be divided into different zones according to the different microstructures: Stirring zone (SZ), Thermomechanically affected zone (TMAZ), Heat affected zone (HAZ) [7, 8]. The microstructures in different welding zones can be affected by many factors including the pin shape, the welding speed, the rotating speed, the shoulder sizes, etc. The mechanical properties of friction stir welding can be obviously affected by the changes of the microstructures in the welding zones, i.e., the hardness [9-11], the tensile strength [12], the fatigue properties [13, 14], the corrosion resistance [15, 16], etc.

Numerical models are important and efficient methods for the investigations on FSW mechanism. A smoothed particle hydrodynamics model was established by Pan et al. [17] to simulate the microhardness and grain sizes in FSW of AZ31. The relations between the Zener-Hollomon parameters and grain size in the stir zone are given. A 3-dimensional numerical analysis model of friction stir welding of copper and aluminum was established by Aalami-Aleagha et al. [18]. The Cellular automata finite element (CAFE) model was used by Saluja et al. [19] to predict the distribution of the grain size during FSW and the effect of welding defects on the forming process of FSW. Manvatkar et al. [20] present a set of easy-to-use maps of cooling rates and peak temperatures for various welding conditions in friction stir welding of high carbon steel. A real time-temperature models for Monte Carlo simulations of normal grain growth were established by Gao et al. [21]. The effect of the tool rotational speed and shoulder penetration depth of friction stir spot welds of aluminum 2024-T3 sheets were studied by Paidar et al. [22]. Buffa et al. [23] investigated the Micro and macro mechanical characteristics of friction stir-welded Ti-6Al-4V lap joints numerically and experimentally. The correlation between microstructure and microhardness in a friction stir welded 2024 aluminum alloy was studied by Jones et al. [24]. A new model related to Zener-Hollomon parameter was originally proposed by Zhang et al. [25] for predictions of grain sizes in friction stir welding of AA2024 alloys. The variations of grain sizes can be directly affected by both temperatures and material flows. An interesting numerical model of material flow behavior was newly proposed by Ji et al. [26]. In recent years, two dimensional MC simulation has been developed to simulate the microstructure evolution in FSW [27, 28]. In comparison with the method for prediction of grain sizes by use of Zener-Hollomon parameter [29, 30], the grain growth process for

*Corresponding author. Tel.: +86 411 84708432, Fax.: +86 411 84708432
E-mail address: zhangz@dlut.edu.cn
† Recommended by Associate Editor Young Whan Park

Table 1. Welding parameters of the simulated cases.

Cases	1	2	3
Rotation speed ω (rpm)	400	1200	400
Shoulder diameter D (mm)	12	12	15
Pin diameter d (mm)	3	3	3

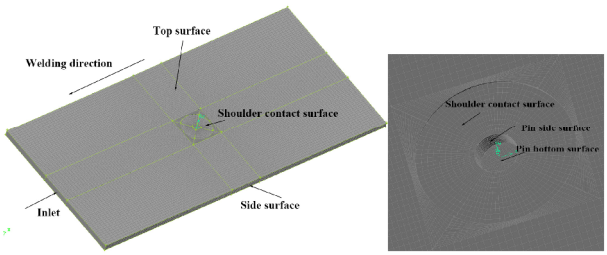

Fig. 1. Finite element model of FSW.

FSW of AA6061 can be directly revealed in detail.

From the literatures mentioned above, it can be found that many interesting models have been successfully developed to investigate different FSW mechanism. But the 3D modelling of grain growth is still lacking. In a Monte Carlo strategy, the energy calculations become more complex in 3D case in comparison with 2D case. So, a 3D Monte Carlo model of grain growth in FSW of AA2024-T3 is newly developed in current work. Furthermore, we studied how the shoulder diameter and rotation speed affect the microstructures in the FSW.

2. Model descriptions

2.1 CFD model of FSW

A Computational fluid dynamics (CFD) model is used to simulate the FSW process. In this work, the material of the welded plate is chosen as AA2024-T3. The thermal properties of AA2024-T3 are considered as functions of temperatures and can be found in Ref. [31].

The dimensions of the aluminum alloy welded plates are 160×75×3 mm. The schematic of CFD model is illustrated in Fig. 1. The inlet velocity is used to represent the transverse speed. Boundary conditions are directly given on the tool-contact surface to define the rotation of the welding tool in CFD model.

The minimum mesh size is 0.24 mm near the welding zone. The welding conditions are summarized in Table 1.

According to Ref. [32], the comparison of laminar and turbulent models shows that the turbulent model can be available for the simulation of FSW process. Moreover, it is found that turbulence model is more suitable for simulation of material flow in welding processes [33]. So, 3D turbulent model is used in current work to simulate the material flow. The calculated temperature on the streamlines are extracted for the further simulation of grain growth in FSW. Detailed information on continuity equation, motion differential equations and energy equation can be found in Ref. [31].

The bottom surfaces and two sides of the plates are assumed to be in contact with the fixed fixtures. Top surface is exposed to the air. The thermal boundary conditions for these surfaces are set as thermal convection according to Ref. [34].

According to Refs. [32, 33, 35], RNG K-ε model is used to predict moderate intensity rotation and low Reynolds number flows. The temperature histories, velocity field and the material flows are calculated by a three-dimensional fluid turbulence model. The turbulent model with k-ε equations based on the renormalization group theory take the rotation effect into account. The low Reynolds number effect can be calculated.

In this CFD model, the relative motion among the welding plate and the tool is represented by the velocity of the inlet. The outflow surface of the plate is free. The solid-state material is regarded as single-phase, incompressible and non-Newtonian fluid during FSW. Viscosity is related to temperature and strain rate and the heat capacity depends on the temperature [31]. Density of workpiece is 2770 kg/m^3 and the thermal conductivity of workpiece is 120 W/m·K. According to Ref. [5], the selection of constant thermal conductivity cannot significantly affect the solutions. The friction heat generated on the interface is given as follows [31],

At the tool shoulder and pin bottom:

$$q_0 = \beta[\delta\tau_y + (1-\delta)\mu_f p_0](r\omega - U\sin\theta)\,. \tag{1}$$

At the pin side:

$$q_1 = \beta[\delta\tau_y + (1-\delta)\mu_f p_0 \sin\alpha](r\omega - U\sin\theta) \tag{2}$$

where p_0 is the pressure at the pin bottom and shoulder, μ_f is the frictional coefficient, and τ_y is the shear yield stress, δ is the slip rate, β is the thermal conversion efficiency, α is the cone angle of the pin, ω is the rotational speed of the tool, U is the welding speed, θ is the angle between a horizontal direction vector from the tool axis to welding direction.

Newtonian viscosity of the material is calculated according to the following formula [36, 37],

$$\mu = \frac{\bar{\sigma}}{3\dot{\bar{\varepsilon}}} \tag{3}$$

where $\dot{\bar{\varepsilon}}$ is the equivalent strain rate, $\bar{\sigma}$ is the equivalent stress of the material [38],

$$\bar{\sigma} = \sqrt{\frac{3}{2}\sigma' : \sigma'} \tag{4}$$

where σ' is the deviatoric stress tensor.

2.2 Microstructure simulation model

In the Monte Carlo model, a 3-D simulation matrix of N×N×N is used for simulation. The orientation numbers Sr, $1 \le Sr \le 30$, are randomly assigned to each lattice point in the matrix. If the orientation of adjacent lattice points is different, it is considered that the two grid points are in the grain bound-

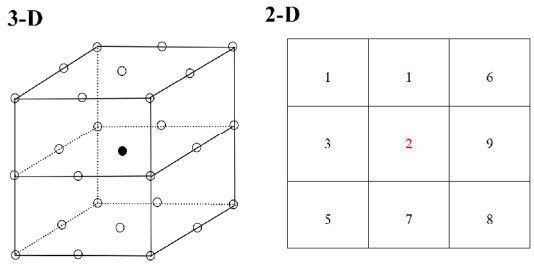

Fig. 2. 3D and 2D energy calculation models.

ary and the grain boundary passes through between two points. The grain-boundary energy for each lattice point can be calculated by the Hamiltonian [33],

$$E = J\sum_{j}^{m}\left(1-\delta_{s_i s_j}\right) \tag{5}$$

where J represents the grain-boundary energy which is a positive constant, m is equal to 26 in this 3-D model, which is the total number of the lattices near the selected points, δ represents the Kronecher function, s_i is the orientation of the calculated grid site and s_j is the orientation of the adjacent lattice point of the calculated grid site.

The calculations of energies for 2D and 3D Monte Carlo models are shown in Fig. 2. In 2D model, the energy is calculated based on the 8 adjacent lattices. For 3D model, the number of the adjacent lattices is increased from 8 to 26. The grain orientation number is also increased. The selection of grain growth direction becomes more complex.

If the energy change $\Delta E \le 0$, the new crystallographic orientation is accepted. If $\Delta E > 0$, the crystallographic orientation will be accepted with the Boltzmann probability [39],

$$p = \begin{cases} 1 & \Delta E \le 0 \\ \exp\left(-\dfrac{\Delta E}{kT}\right) = \exp\left(-J\dfrac{n_2-n_1}{kT}\right) & \Delta E > 0 \end{cases} \tag{6}$$

where T is the temperature while k represents the Boltzmann constant, n_1 is the number of the orientation before the reorientation, n_2 is the number of the orientation after the reorientation.

The above algorithm iterates N^3 times in a MC step. The orientation matrix represents the microstructure in the Monte Carlo model. The average grain size is calculated by the following formula,

$$L = \sqrt[3]{\frac{V}{\mathrm{n_g}}} \tag{7}$$

where V is the volume of this simulation and $\mathrm{n_g}$ is the grain number in the simulated area. The empirical fitting relationship between the MC steps number and the grain size is as follows [36],

$$L = K_1\lambda(MCS)^{n_1} \tag{8}$$

where λ is the lattice spacing of the model, K_1 and n_1 are the constants of the model which can be obtained by regression analysis of the simulated data.

In the current work, the rate of change of the average grain size is considered as a function of the grain boundary migration velocity (v) [36],

$$\frac{dL}{dt} = \alpha v^n \tag{9}$$

where α is chosen as 1.0 and n is chosen as 0.49, all of them are ratio constants. Choosing the reasonable equation constants can lead to the grain growth kinetics conforming to the real grain growth. The movement of grain boundaries drives the real growth of the grain and v is defined as [21],

$$v = \frac{AZV_m^2}{N_a^2 h}\exp\left(\frac{\Delta S_f}{R}\right)\exp\left(-\frac{Q}{RT}\right)\left(\frac{2\gamma}{r}\right) \tag{10}$$

where A, Z, V_m, R, h and N_a are physical constants. γ and ΔS_f are material parameters of AA2024-T3. The ratio constants and material parameters of AA2024-T3 used in Eqs. (9) and (10) are summarized in Table 2 [40-42].

Table 2. Parameters used in the simulation [40-42].

Physical property	Value
Average number per unit area, Z/atoms·m^{-2}	4.31×10^{20} atoms/m^2
Accommodation probability, A	1.0
Planck's constant, h	6.624×10^{-34} J s
Avogadro's number, N_a	6.02×10^{23} /mol
Fusion entropy, ΔS_f	11.5 J/mol·K^{-1}
Activation enthalpy, Q	148.9 KJ/mol
Boundary energy, γ	0.5 J/m^2
Gas constant, R	8.31 J/mol·K^{-1}
Ratio constant, α	1
Ratio constant, n	0.49

From Eqs. (8)-(10), the relationship between the simulation time and the MC steps can be derived as follows:

$$(MCS^{(n+1)n_1}) = \left(\frac{L_0}{K_1\lambda}\right)^{n+1} + \frac{(n+1)\alpha C_1^n}{(K_1\lambda)^{n+1}}\sum\left[\exp^n\left(-\frac{Q}{RT_i}\right)t_i\right] \tag{11}$$

where $C_1 = \dfrac{2A\gamma ZV_m^2}{N_a^2 h}\exp\left(\dfrac{\Delta S_f}{R}\right)$, T_i is the average temperature in every time interval, L_0 is the average grain size of the initial and t_i represents the time interval value.

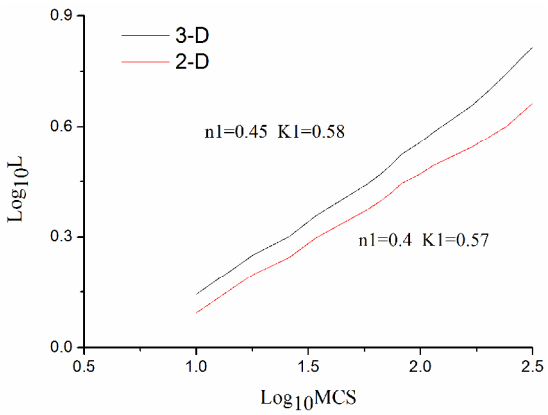

Fig. 3. Relations between Log10MCS and Log10L in SZ.

The welding area is a region with high temperature and obvious plastic deformation. Therefore, in the grain growth simulation the Dynamic recrystallization (DRX) should be take into consideration. In this model, DRX process is realized by distribution of seeds in each MC step. The nucleation rate can be regarded as the function of the strain rate and the temperature [40],

$$\dot{n} = N_0 \dot{\bar{\varepsilon}} \exp\left(-\frac{Q}{RT}\right) \tag{12}$$

where N_0 is taken as $10^{24}(1/s/m^3)$ which is a constant, $\dot{\bar{\varepsilon}}$ is assumed to be uniform in SZ, which represents the equivalent strain rate and can be estimated through the equation [38],

$$\dot{\bar{\varepsilon}} = \frac{w\pi r_e}{L_e} \tag{13}$$

where L_e and r_e are the average depth and radius of the SZ, respectively. r_e here is 0.78, and L_e can be taken as the pin length. From the rate of nucleation to calculate the number of nuclei, and lattice points are chosen to create new nuclei at grain boundary. It is obvious that the nucleation rate changes with the change of temperature and equivalent strain rate during the simulation.

3. Results and discussions

3.1 Validation of numerical models

The simulated area is 50×50×50 μm^3, and the grid system is 120×120×120. The relation between the grain growth and the MCS is shown in Fig. 3. It can be seen that the grain growth exponent for 2D MC model is 0.4. For 3D MC model, the grain growth exponent is increased to 0.45. The grain growth exponent in 3D model is much closer to 0.5, which is the ideal grain growth exponent. The grain growth exponent shown in Fig. 3 can be an efficient criterion to show the validity of the proposed Monte Carlo model. So, the comparison of 2D MC model and 3D MC model shows that 3D MC model is much more accurate for simulations of grain growth.

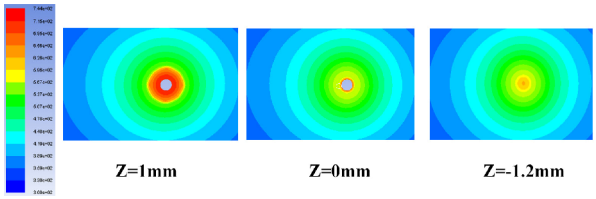

Fig. 4. Temperature distributions in Case 1.

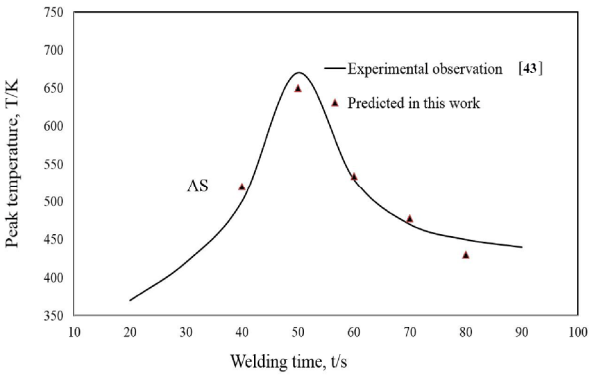

Fig. 5. Temperature validation in 400 rpm.

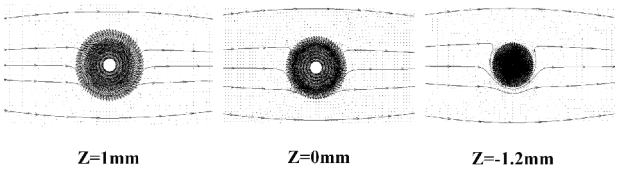

Fig. 6. Streamlines in Case 1.

To further validate the proposed model, a new case is selected for comparison of grain sizes in both experimental and numerical results with same welding parameters. The maximum temperature is 744 K when the rotation speed is 400 rpm as shown in Fig. 4. The welding temperature near the top surface is much higher than the bottom surface. This means that in friction stir welding, the shoulder can play a major role in heat production. This phenomenon has been studied in previous work theoretically [38]. The calculated temperature is in good agreement with the experimental results in Ref. [43]. The errors between the maximum temperature obtained from the simulation is less than 0.5 % compared with the data obtained from the experiment.

In order to obtain the temperature curves, 300 points in numerical model are extracted from each stream lines. The data are used to calculate the MC steps by Eq. (11). The streamlines of this case are shown in Fig. 6. Then in the further MC simulations, the grain sizes can be obtained. Moreover, the predicted grain sizes by use of 3D MC model is further compared with experimental data in FSW, as shown in Table 3. The comparisons between the experimental data and the predicted grain sizes shows that the computational results from the proposed 3D turbulence model and the 3D Monte Carlo

Table 3. Validation of DRX simulation in SZ.

	Measured (μm) [43]	Simulated (μm)	Error (%)
Case 1	2.6	2.8	7.6

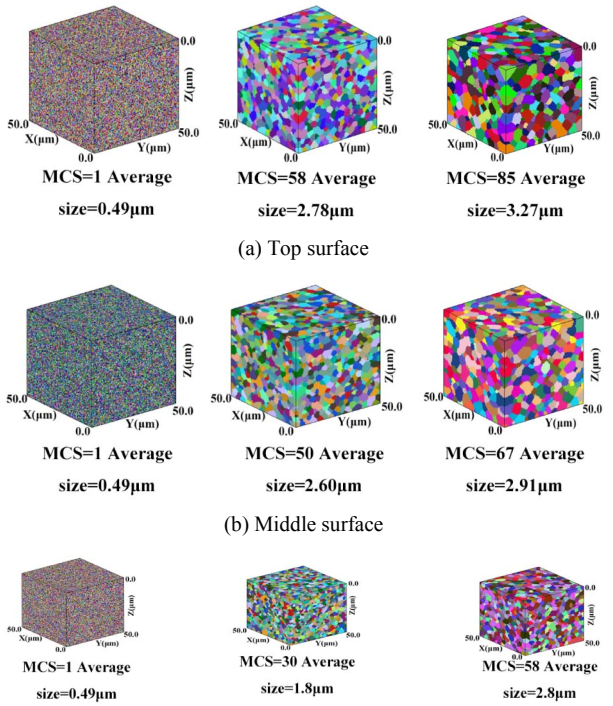

Fig. 7. Simulated grain growth process of stirring zone from top to bottom surfaces in Case 1.

model can agree well with the experimental tests.

3.2 Case 1: ω = 400 rpm, v = 50 mm/min, D = 12 mm

The material flows in different depths in this case have been shown and discussed in Fig. 6. It is obvious that near the top surface the material flow can be significantly affected by the shoulder. For the material outside of the shoulder region, stirring effect from the shoulder becomes weaker. The calculated grain sizes and the grain growth process in different depths are shown in Fig. 7. The grain size on the top surface is larger than the bottom surface. This phenomenon is fitted well with numerical observation from Ref. [31], which can also validate the current model for predictions of material flows. Along the streamline shown in Fig. 6, the material particles can be heated and cooled. Recrystallization occurs in this process [43-45]. As shown in both experimental and numerical works [46-48], the flowing behaviors of material particles in the stirring zone can be different. The different streamlines can lead to different heating and cooling curves, which can lead to different grain growth processes at different locations. At the advancing side, with the effect of the tool, the material can flow into the retreating side, which is fitted well with both the experimental [4] and numerical [6] observations. The extrusion phenomenon can be observed at the retreating side [31].

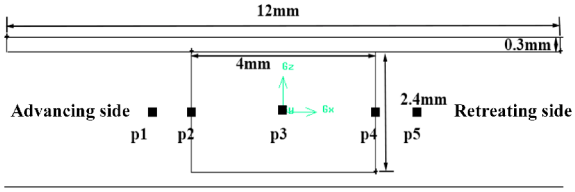

Fig. 8. The position of different point from AS to RS in Case 1.

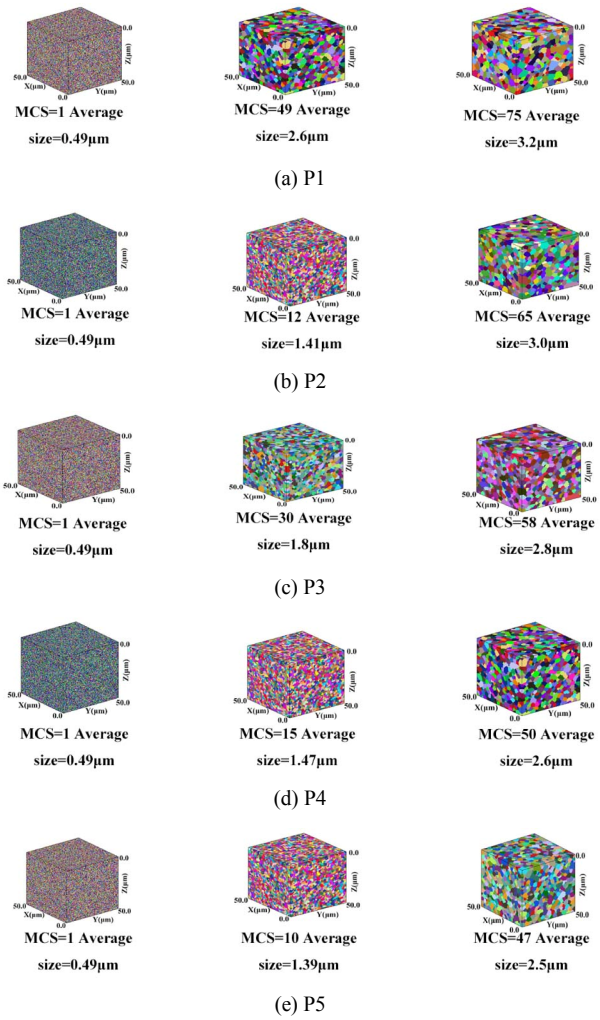

Fig. 9. Simulated grain growth process of stir zone in the middle regions from AS to RS in Case 1.

From the equations for MC simulation, it can be seen that temperature history is very important for the grain growth in the friction stir welding process. Higher temperature can lead to larger grains. So, larger grains can be generally found near the shoulder-contact surface. This phenomenon is fitted well with the experimental observations from Chang et al. [49].

To further reveal the grain distributions in the stirring zone in FSW, 5 points are selected in the middle surface to calculate the grain sizes, as shown in Fig. 8. The grain growth at different locations is shown in Fig. 9 and then is further sum-

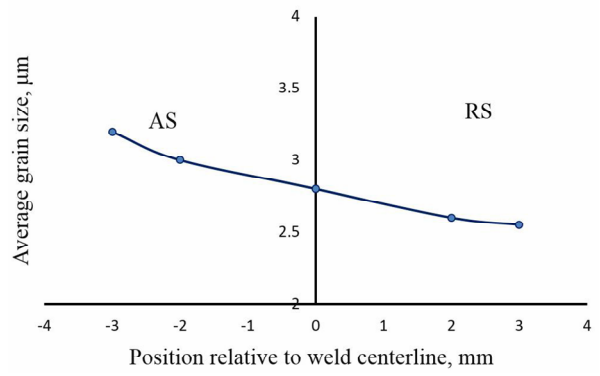

Fig. 10. Predicted grain sizes at different locations in Case 1.

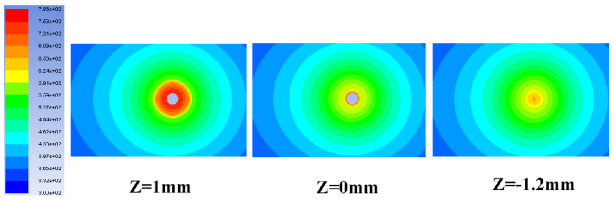

Fig. 11. Temperature distributions in Case 2.

marized in Fig. 10. It is obvious that there is a difference between the average grain sizes on both advancing and retreating sides. The different grain sizes on both advancing and retreating sides are caused by the different material flows and then the corresponding different temperature histories of particles in FSW. Longer high temperature history can lead to the larger grains. From the flowing streamlines, it is easy to see that the history of the high temperature at the advancing side is longer than the retreating side. So, the predicted grain sizes at the advancing side are larger than the retreating side.

3.3 Case 2: ω = 1200 rpm, v = 50 mm/min, D = 12 mm

To investigate the effect of rotation speed, a new case with rotation speed of 1200 rpm (Case 2) is selected from comparison. The maximum temperature of the welding is increased to 786 K as the rotation speed increased to 1200 rpm, as shown in Fig. 11. In comparison with Case 1, the maximum welding temperature is increased by 42 K. As the rotation speed increases, the welding temperature is also increased, which has been validated by other articles [6, 43]. On the top surface, the maximum welding temperature is 721 K. On the bottom, the maximum temperature of the welding is 683 K. The maximum temperature on the bottom surface is increased by 33 K in comparison with Case 1.

In order to obtain the microstructures, 300 points in numerical model are selected to extract the temperature curves from each stream lines. The streamlines of this case are shown in Fig. 12. The streamlines area and the revealed flow patterns are similar to Case 1 but the time—temperature history is different.

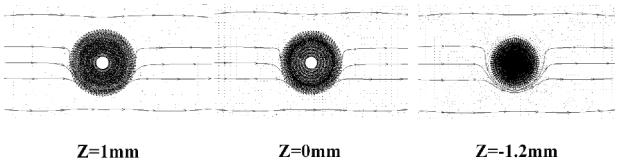

Fig. 12. Streamlines in Case 2.

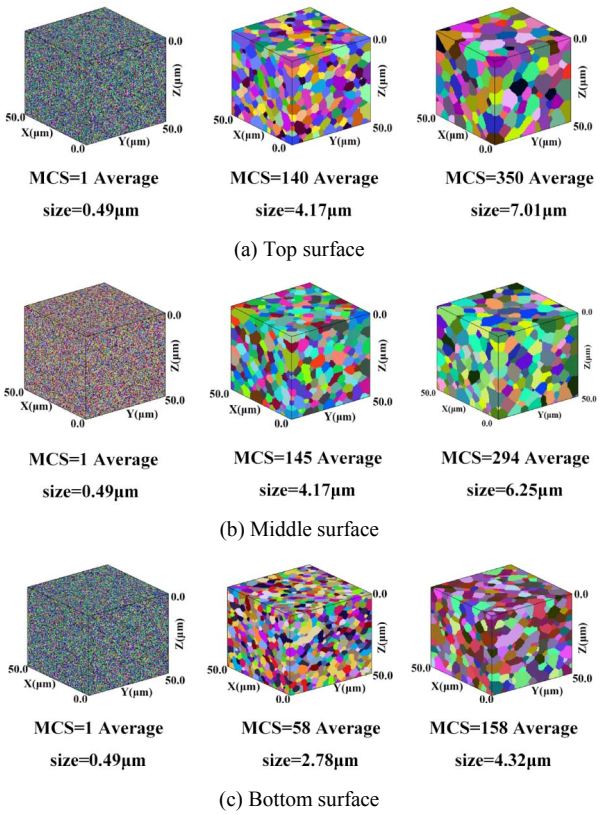

Fig. 13. Simulated grain growth process of stirring zone from top to bottom surfaces in Case 2.

Fig. 13 shows the grain growth processes from top to bottom surfaces in Case 2. When the rotation speed is increased from 400 rpm to 1200 rpm, the average grain sizes are simultaneously increased from 3.27 μm, 2.91 μm and 2.47 μm to 7.01 μm, 6.25 μm and 4.32 μm on the top, middle and bottom surfaces, respectively. With the increase of the rotational speed, the average grain size increases, which can be observed in many experimental tests [43, 45]. In comparison with Case 1, the difference in grain sizes between the bottom and the top surfaces becomes larger.

The grain growth at different locations in the middle surface are shown in Fig. 14 and then is further summarized in Fig. 15. Obviously, the average grain sizes on both the retreating and the advancing sides are different. This is caused by the longer high temperature of the flowing particles on the streamlines on the advancing side, which can be easily observed from the streamlines as shown in Fig. 12. On the advancing side, the maximum grain size is 7.10 μm. On the retreating side, the

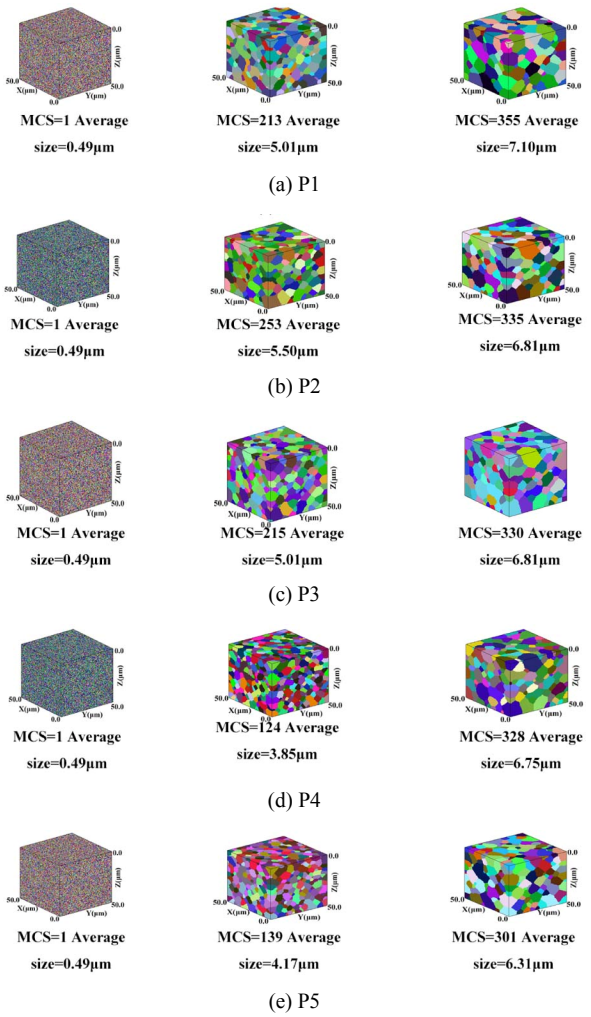

Fig. 14. Simulated grain growth process of stir zone in the middle surface from AS to RS in Case 2.

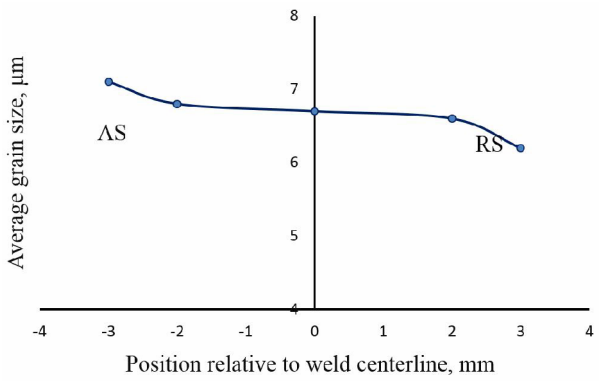

Fig. 15. Predicted grain sizes at different locations in Case 2.

grain size is decreased to 6.31 μm at the same distance from the welding line. In comparison with Case 1, as the rotational speed increases, the average grain size is increased. But the differences of the grain sizes between the advancing and re-treating sides becomes smaller.

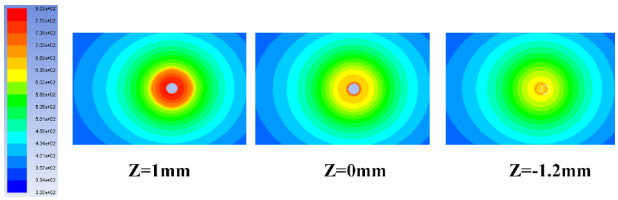

Fig. 16. Temperature distributions in Case 3.

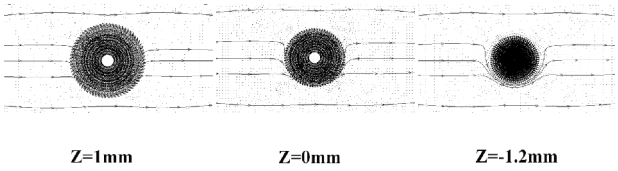

Fig. 17. Streamlines in Case 3.

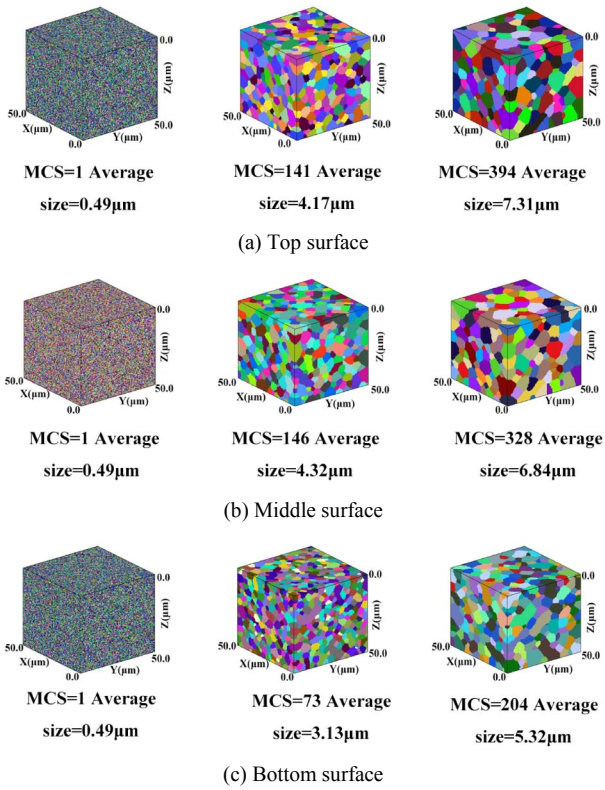

Fig. 18. Simulated grain growth process of stirring zone from top to bottom surfaces in Case 3.

3.4 Case 3: ω = 400 rpm, v = 50 mm/min, D = 15 mm

With the diameter of the shoulder is increased from 12 mm to 15 mm, the maximum temperature of the welding can be increased to 803 K, as shown in Fig. 16. In comparison with Case 1, the welding temperature is increased by 59 K. On the bottom surface, the maximum welding temperature is 708 K. In comparison with Case 1, the temperature is increased by 55 K on the bottom surface.

From the streamlines shown in Figs. 17 and 6, it can be seen that the welding region becomes larger when the shoulder size

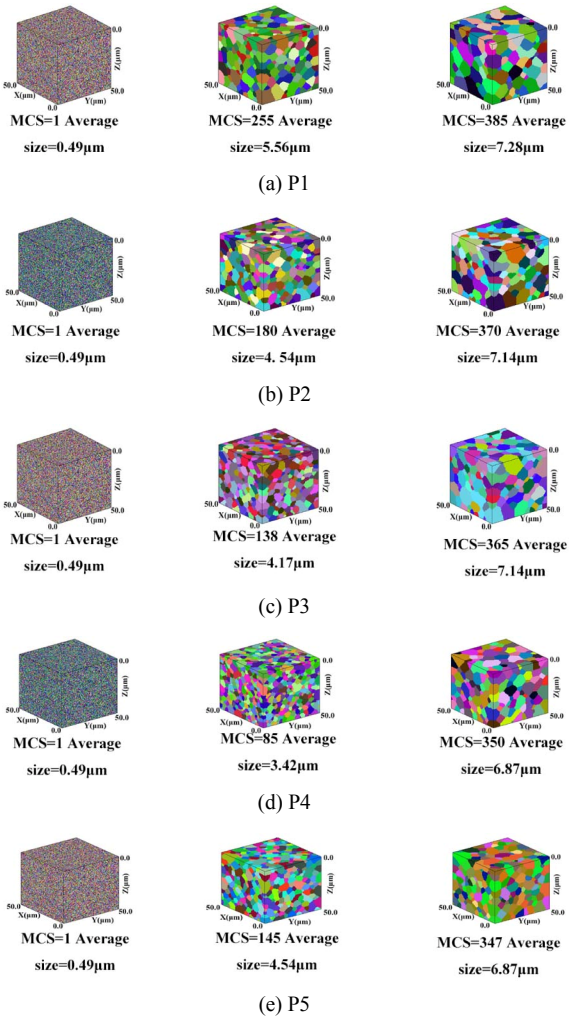

Fig. 19. Simulated grain growth process of stir zone in the middle surface from AS to RS in Case 3.

is increased.

Fig. 18 shows the grain growth processes from top to bottom surface in Case 3. When the shoulder diameter is increased from 12 mm to 15 mm, the average grain size from top to bottom surface in Case 3 are simultaneously increased from 3.27 μm, 2.91 μm and 2.47 μm to 7.31 μm, 6.84 μm and 5.32 μm on the top, middle and bottom surfaces, respectively. The difference of grain sizes between the top and the bottom surfaces becomes larger compared with Case 1. The increases of the shoulder diameter can cause higher heat input at the same time increment which can lead to higher peak welding temperature [50]. Higher temperature can lead to the increase of the grain sizes in the stirring zone [29]. So, with the increase of the shoulder diameter, the average grain size is increased.

The grain size distributions at different locations on the middle surface in Case 3 are shown in Fig. 19 and are summarized in Fig. 20. The maximum grain size occurs on the advancing side due to higher experienced temperature. So, the maximum grain size on the middle surface is increased from

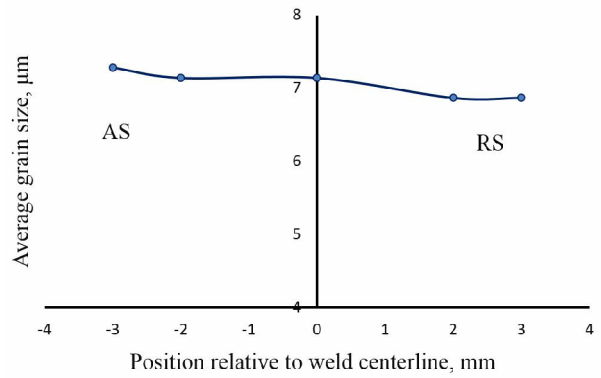

Fig. 20. Predicted grain sizes at different locations in Case 3.

3.2 μm to 7.28 μm. But at the same distance from the welding line in Case 3, the grain size is 6.87 μm. In comparison with Case 1, with the increase of the shoulder diameter, the grain sizes on advancing and retreating sides are both increased. The grain size in the stirring zone tends to be more uniform from retreating side to advancing side with the increase of shoulder diameter on middle surface.

4. Conclusions

(1) In comparison with 2D Monte Carlo model, the new proposed 3D Monte Carlo model is much more accurate for predictions of grain growth in friction stir welding.

(2) With the increase of the rotation speed, the average grain size is increased and the grains tend to be more uniform from advancing side to retreating side.

(3) With the increase of the shoulder diameter, the welding zone can be increased and the average grain size is also increased due to the higher welding temperature.

Acknowledgment

This work was supported by the National Natural Science Foundation of China (Nos. 11572074 and 11172057).

References

[1] R. S. Mishra and Z. Y. Ma, Friction stir welding and processing, *Materials Science and Engineering R*, 50 (1-2) (2005) 1-78.

[2] R. Nandan, T. DebRoy and H. Bhadeshia, Recent advances in friction-stir welding-process, weldment structure and properties, *Progress in Materials Science*, 53 (6) (2008) 980-1023.

[3] M. Guerra, C. Schmidt, J. C. McClure, L. E. Murr and A. C. Nunes, Flow patterns during friction stir welding, *Materials Characterization*, 49 (2003) 95-101.

[4] S. Muthukumaran and S. K. Mukherjee, Multi-layered metal flow and formation of onion rings in friction stir welds, *International Journal of Advanced Manufacturing Technology*, 38 (2008) 68-73.

[5] Z. Zhang and J. T. Chen, Computational investigations on

reliable finite element based thermo-mechanical coupled simulations of friction stir welding, *International Journal of Advanced Manufacturing Technology*, 60 (2012) 959-975.

[6] Z. Zhang and H. W. Zhang, Numerical studies on controlling of process parameters in friction stir welding, *Journal of Materials Processing Technology*, 209 (1) (2009) 241-270.

[7] L. H. Wu, D. Wang, B. L. Xiao and Z. Y. Ma, Microstructural evolution of the thermomechanically affected zone in a Ti-6Al-4V friction stir welded joint, *Scripta Materialia*, 78 (2014) 17-20.

[8] Y. C. Chen, J. C. Feng and H. J. Liu, Precipitate evolution in friction stir welding of 2219-T6 aluminum alloys, *Materials Characterization*, 60 (6) (2009) 476-481.

[9] E. A. El-Danaf and M. M. El-Rayes, Microstructure and mechanical properties of friction stir welded 6082 AA in as welded and post weld heat treated conditions, *Materials & Design*, 46 (2013) 561-572.

[10] M. M. Attallah, C. L. Davis and M. Strangwood, Microstructure-microhardness relationships in friction stir welded AA5251, *Journal of Materials Science*, 42 (17) (2007) 7299-7306.

[11] T. Sakthivel and J. Mukhopadhyay, Microstructure and mechanical properties of friction stir welded copper, *Journal of Materials Science*, 42 (19) (2007) 8126-8129.

[12] M. Jayaraman and V. Balasubramanian, Effect of process parameters on tensile strength of friction stir welded cast A356 aluminium alloy joints, *Transactions of Nonferrous Metals Society of China*, 23 (3) (2013) 605-615.

[13] K. Sillapasa, S. Surapunt, Y. Miyashita, Y. Mutoh and N. Seo, Tensile and fatigue behavior of SZ, HAZ and BM in friction stir welded joint of rolled 6N01 aluminum alloy plate, *International Journal of Fatigue*, 63 (2014) 162-170.

[14] M. D. Giorgi, A. Scialpi, F. W. Panella and L. A. C. D. Filippis, Effect of shoulder geometry on residual stress and fatigue properties of AA6082 FSW joints, *Journal of Mechanical Science and Technology*, 23 (1) (2009) 26-35.

[15] K. P. Rao, G. D. J. Ram and B. E. Stucker, Improvement in corrosion resistance of friction stir welded aluminum alloys with micro arc oxidation coatings, *Scripta Materialia*, 58 (11) (2008) 998-1001.

[16] Y. Yang and L. Zhou, Improving corrosion resistance of friction stir welding joint of 7075 aluminum alloy by micro-arc oxidation, *Journal of Materials Science and Technology*, 30 (12) (2014) 1251-1254.

[17] W. Pan, D. Li, A. M. Tartakovsky, S. Ahzi, M. Khraisheh and M. Khaleel, A new smoothed particle hydrodynamics non-Newtonian model for friction stir welding: Process modeling and simulation of microstructure evolution in a magnesium alloy, *International Journal of Plasticity*, 48 (2013) 189-204.

[18] M. E. Aalami-Aleagha, B. Hadi and M. A. Shahbazi, 3-dimensional numerical analysis of friction stir welding of copper and aluminum, *Journal of Mechanical Science and Technology*, 30 (8) (2016) 3767-3776.

[19] R. S. Saluja, R. G. Narayanan and S. Das, Cellular automata finite element (CAFE) model to predict the forming of friction stir welded blanks, *Computational Materials Science*, 58 (2012) 87-100.

[20] V. Manvatkar, A. De, L. E. Svensson and T. DebRoy, Cooling rates and peak temperatures during friction stir welding of a high-carbon steel, *Scripta Materialia*, 94 (2015) 36-39.

[21] J. H. Gao and R. G. Thompson, Real time-temperature models for Monte Carlo simulations of normal grain growth, *Acta Materialia*, 44 (11) (1996) 4565-4570.

[22] M. Paidar, A. Khodabandeh, H. Najafi and A. S. Rouh-Aghdam, Effects of the tool rotational speed and shoulder penetration depth on mechanical properties and failure modes of friction stir spot welds of aluminum 2024-t3 sheets, *Journal of Mechanical Science and Technology*, 28 (12) (2014) 4893-4898.

[23] G. Buffa, L. Fratini, M. Schneider and M. Merklein, Micro and macro mechanical characterization of friction stir welded Ti-6Al-4V lap joints through experiments and numerical simulation, *Journal of Materials Processing Technology,* 213 (12) (2013) 2312-2322.

[24] M. J. Jones, P. Heurtier, C. Desrayaud, F. Montheillet, D. Allehaux and J. H. Driver, Correlation between microstructure and microhardness in a friction stir welded 2024 aluminium alloy, *Scripta Materialia*, 52 (8) (2005) 693-697.

[25] Z. H. Zhang, W. Y. Li, J. L. Li and Y. J. Chao, Effective predictions of ultimate tensile strength, peak temperature and grain size of friction stir welded AA2024 alloy joints, *The International Journal of Advanced Manufacturing Technology*, 73 (2014) 1213-1218.

[26] S. D. Ji, Q. Y. Shi, L. G. Zhang, A. L. Zou, S. S. Gao and L. V. Zan, Numerical simulation of material flow behavior of friction stir welding influenced by rotational tool geometry, *Computational Materials Science*, 63 (2012) 218-226.

[27] Z. Zhang, Q. Wu, M. Grujicic and Z. Y. Wan, Monte Carlo simulation of grain growth and welding zones in friction stir welding of AA6082-T6, *Journal of Materials Science*, 51 (2016) 1882-1895.

[28] M. Grujicic, S. Ramaswami, J. S. Snipes, V. Avuthu, R. Galgalikar and Z. Zhang, Prediction of the grain-microstructure evolution within a Friction stir welding (FSW) joint via the use of the Monte Carlo simulation method, *Journal of Materials Engineering and Performance*, 24 (2015) 3471-3486.

[29] Z. Zhang and Q. Wu, Numerical studies of tool diameter on strain rates, temperature rises and grain sizes in friction stir welding, *Journal of Mechanical Science and Technology*, 29 (10) (2015) 4121-4128.

[30] Z. Y. Wan, Z. Zhang and X. Zhou, Finite element modeling of grain growth by point tracking method in friction stir welding of AA6082-T6, *The International Journal of Advanced Manufacturing Technology,* 90 (2017) 3567-3574.

[31] H. Su, C. S. Wu, A. Pittner and M. Rethmeier, Thermal energy generation and distribution in friction stir welding of aluminum alloys, *Energy*, 77 (2014) 720-731.

[32] A. K. Kadian and P. Biswas, A comparative study of material flow behavior in friction stir welding using laminar and turbulent models, *Journal of Materials Engineering and Performance*, 24 (10) (2015) 4119-4127.

[33] Z. Yang, S. Sista, J. W. Elmer and T. Debroy, Three dimensional Monte Carlo simulation of grain growth during GTA welding of titanium, *Acta Materialia*, 48 (20) (2000) 4813-4825.

[34] M. Riahi and H. Nazari, Analysis of transient temperature and residual thermal stresses in friction stir welding of aluminum alloy 6061-T6 via numerical simulation, *The International Journal of Advanced Manufacturing Technology*, 55 (1) (2011) 143-152.

[35] Z. Zhang, Q. Wu and H. W. Zhang, Prediction of fatigue life of welding tool in friction stir welding of AA6061-T6, *The International Journal of Advanced Manufacturing Technology*, 9 (86) (2016) 3407-3415.

[36] Z. Zhang and Q. Wu, Prediction of tool fatigue life in friction stir welding, *International Journal of Advanced Manufacturing Technology*, 86 (9) (2016) 3407-3415.

[37] Z. Zhang and Q. Wu, Analytical and numerical studies of fatigue stresses in friction stir welding, *International Journal of Advanced Manufacturing Technology*, 78 (2015) 1371-1380.

[38] Z. Zhang and H. W. Zhang, Solid mechanics-based Eulerian model of friction stir welding, *International Journal of Advanced Manufacturing Technology*, 72 (2014) 1647-1653.

[39] C. M. Huang, C. L. Joanne, B. S. V. Patnaik and R. Jayaganthan, Monte Carlo simulation of grain growth in polycrystalline materials, *Applied Surface Science*, 252 (11) (2006) 3997-4002.

[40] G. W. Driver and K. E. Johnson, Interpretation of fusion and vaporisation entropies for various classes of substances, with a focus on salts, *The Journal of Chemical Thermodynamics*, 70 (2014) 207-213.

[41] C. C. Yang, A. D. Rollett and W. W. Mullins, Measuring relative grain boundary energies and mobilities in an aluminum foil from triple junction geometry, *Scripta Materialia*, 44 (12) (2001) 2735-2740.

[42] D. M. Kirch, E. Jannot, L. A. Barrales-Mora, D. A. Molodov and G. Gottstein, Inclination dependence of grain boundary energy and its impact on the faceting and kinetics of tilt grain boundaries in aluminum, *Acta Materialia*, 56 (18) (2008) 4998-5011.

[43] S. A. Khodir, T. Shibayanagi and M. Naka, Microstructure and mechanical properties of friction stir welded AA2024-T3 aluminum alloy, *Materials Transactions*, 47 (1) (2006) 185-193.

[44] R. Ding and Z. X. Guo, Coupled quantitative simulation of microstructural evolution and plastic flow during dynamic recrystallization, *Acta Materialia*, 49 (16) (2001) 3163-3175.

[45] Y. S. Sato, M. Urata and H. Kokawa, Parameters controlling microstructure and hardness during friction-stir welding of precipitation-hardenable aluminum alloy 6063, *Metallurgical and Materials Transactions A*, 33 (3) (2002) 625-635.

[46] Z. Zhang and J. T. Chen, Computational investigations on reliable finite element-based thermomechanical-coupled simulations of friction stir welding, *The International Journal of Advanced Manufacturing Technology*, 60 (9-12) (2012) 959-975.

[47] Z. Zhang and H. W. Zhang, Numerical studies of preheating time effect on temperature and material behaviours in friction stir welding process, *Science and Technology of Welding & Joining*, 12 (5) (2007) 436-448.

[48] A. Tongne, C. Desrayaud, M. Jahazi and E. Feulvarch, On material flow in friction stir welded Al alloys, *Journal of Materials Processing Technology*, 239 (2017) 284-296.

[49] C. I. Chang, C. J. Lee and J. C. Huang, Relationship between grain size and Zener-Holloman parameter during friction stir processing in AZ31 Mg alloys, *Scripta Materialia*, 51 (6) (2004) 509-514.

[50] A. F. Norman, I. Brough and P. B. Prangnell, High resolution EBSD analysis of the grain structure in an AA2024 friction stir weld, *Materials Science Forum*, 331 (2000) 1713-1718.

Zhao Zhang, Ph.D., is a Professor in Department of Engineering Mechanics at Dalian University of Technology. He received his doctoral degree from Dalian University of Technology in 2007. He is a member of International Association of Computational Mechanics and serves as reviewers for about 20 international journals. His scientific research is focused on numerical simulation of friction stir welding, safety design of locomotive, and fracture mechanics. He published about 100 articles and 3 books with more than 900 citations (Including 40 SCI indexed articles with more than 500 SCI citations).